

# Optimizing the Bandpasses of a High Resolution Spectrophotometer for Characterizing Hot Jupiter Atmospheres

UZAIR TAHAMID SIAM,<sup>1</sup> ASHLEY BAKER,<sup>2</sup> DIMITRI MAWET,<sup>2</sup> ANDREW HOWARD,<sup>2</sup> NEMANJA JOVANOVIC,<sup>2,3</sup> AND SAM HALVERSON<sup>4</sup>

<sup>1</sup> University of Rochester, 500 Joseph C Wilson Blvd, Rochester, NY-14627

<sup>2</sup> California Institute of Technology Department of Astronomy, 1200 E California Blvd, Pasadena, CA 91125

<sup>3</sup> California Optical Observatories

<sup>4</sup> Jet Propulsion Laboratory, Pasadena CA

(Received November 10, 2019; Revised December 26, 2019; Accepted December 29, 2019)

Submitted to ApJS

## ABSTRACT

Studying exoplanet atmospheres give us insight into the composition of exoplanets as well as habitability. Existing multi-object spectrographs are commonly used for medium-resolution transit spectroscopy observations; however, these instruments are not optimally efficient and often are affected by instrument systematics that are difficult to calibrate out of the data. The High-efficiency Instrument for Rapid Assessment of eXo-atmosphere (HIRAX) is an upcoming instrument for Palomar that can image a star in multiple high throughput, narrow bandpasses achieving  $R \sim 2000$ , and is being specifically designed for atmospheric characterization of exoplanets. In this paper, we describe work simulating HIRAX observations to understand the optimal choice of the instrument's five bandpasses, including their center wavelengths and bandwidths in order to detect sodium in transiting Hot Jupiter atmospheres. We present the results of signal-to-noise ratio calculations describing the expected sodium detection achievable for host stars of varying magnitudes for the various bandpass configurations as well as estimations of the number of confirmed exoplanets that could be characterized for each configuration. Finally, we will show the effects of Doppler shifts on the exoplanet spectrum with respect to the static HIRAX bands due to various system velocities and how the band placements overlap with characteristic features of the Earth's atmosphere.

*Keywords:* exoplanet atmospheres, instrumentation, transit spectrophotometry

## 1. INTRODUCTION

Exoplanets are planets outside the Solar System. The first of its kind was detected in 1992 around a pulsar but in 1995 the first exoplanet around a sun-like star was discovered and given the name 51 Pegasi B. Since then, more than 4000 have been found. Of the 4000 detected, the highest fraction of exoplanets has been Hot Super-Earths followed very closely by Hot Jupiters<sup>1</sup>. There are various methods used to discover exoplanets; the transit method has by far been the most effective and widely used since 2007. During a transit, as a planet orbits around its host star, the planet eclipses its host and

during this process the star's flux that is detected by an observer on Earth decreases. By measuring the dip in flux we can learn about the properties of the planet including the planet radius and, if measured as a function of wavelength, the planet's atmosphere.

The atmosphere of a planet allows us to study the chemical composition alongside the thermal properties of the planet. Transit spectroscopy (Knutson et al. 2014) allows us to characterize these atmospheres. Fig. 1 shows a simplified schematic of how the spectroscopy works. There is a change in radius of the planet that can be observed due to the changing opacity of the atmosphere as a function of different wavelengths as a planet orbits the host star. Using this change we can identify the characteristic elements that are present in the atmosphere and responsible for the change in radius. Sodium is an element that has been discovered

Corresponding author: Ashley Baker  
[abaker@caltech.edu](mailto:abaker@caltech.edu)

<sup>1</sup> <http://phl.upr.edu/projects/habitable-exoplanets-catalog/media/>

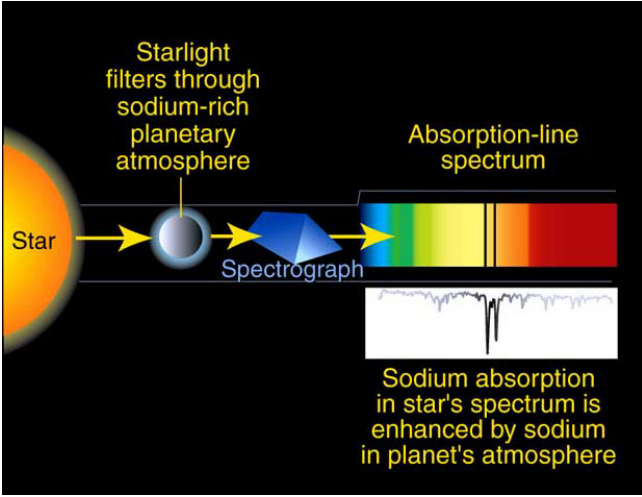


**Figure 1.** Summary of how the process of transit spectroscopy. Sodium filters out light from its parent star, and is detected using by analyzing absorption spectrum. Credit: A. Field, STScI

in many Hot Jupiter atmospheres (e.g. Fisher & Heng 2019), and can inform of the temperature, pressure, and cloud content of an exoplanet (Heng 2016).

While studying exoplanetary atmospheres can give us a lot of information, there are no dedicated instruments optimized for studying exoplanetary atmospheres. Currently, most medium resolution transit spectroscopy measurements are done from space telescopes. The ground-based instruments that are used for transit spectroscopy are existing multi-object grating-based spectrographs that are affected by systematics and contamination from Earth's atmosphere and had not been designed to meet the photometric precision requirements for exoplanet spectroscopy applications. However, our largest telescopes are our ground-based telescopes that not only offer more telescope time, but also optical coverage - something we will soon lose from space-based telescopes as the Hubble mission comes to an end.

Recently, Baker et al. (2019) proposed a multiband imager for transit spectrophotometric measurements that they showed reaches near the photon noise limit on sky in their two adjacent ultranarrow bandpasses. The design is based on Fabry Perot filters that offer a resolving power of  $R \sim 2000$  around 600 nm. They proposed the instrument design and calculations for ground or space-based measurements assuming future large aperture telescopes to characterize the oxygen A band in Earth-like exoplanet atmospheres. They also suggested the current application to hot Jupiter atmospheres, which are already accessible to today's telescopes. Here, we are interested in studying the optimal band placement of a similar instrument we call the High-efficiency Instru-

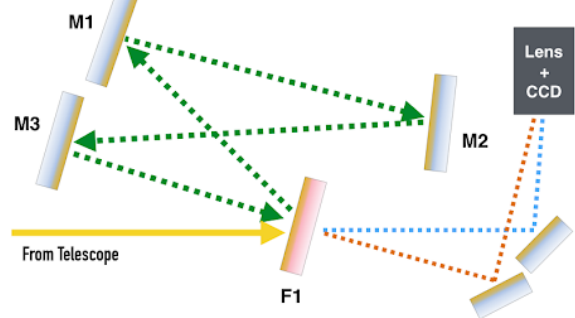


**Figure 2.** Schematic of a possible optical configuration for HIRAX. A collimated beam from the telescope is passed through a narrowband (0.3 nm bandwidth) filter, F1, at an angle, causing a blue-shifted bandpass profile due to the wavelength sensitivity of the filter to incidence angles away from normal. Out-of-bandpass light is reflected off of F1, redirected by a series of mirrors, and then is passed through F1 at normal incidence. In this way, images of a star can be taken simultaneously in two narrow bands. A design that achieves 3-5 bandpasses is being studied in separate work; here we are interested in optimizing the central wavelength and bandwidths of the HIRAX bandpasses. Taken from (Baker et al. 2019).

ment for the Rapid Assessment of eXo-atmospheres, or HIRAX, in order to optimally detect the sodium feature in hot Jupiter atmospheres. HIRAX is an instrument being designed to operate at the prime focus of the Hale Telescope at Palomar Observatory.

HIRAX achieves source images over multiple narrow bands (on the order of Angstroms in width). Fig. 2 shows an example instrument design for HIRAX. The filter bands shown are very high throughput so they enable efficient photometry while maintaining high resolution, which is ideal for atmospheric characterization.

This work presented here is one step in investigating new technologies for studying exoplanet atmospheres: choosing the optimal bandpasses for HIRAX and assessing its basic noise properties. Investigating the application of such a novel instrument for exoplanet science and exploring its capabilities could present an important path forward for ground-based exoplanet characterization efforts of Hot Jupiters. In the future space-based missions could adopt a HIRAX-like instrument which could allow characterization of Terrestrial planets in the hopes of finding biosignatures.

This paper is structured as follows. In §2 we describe the source of the models used in the simulations and the assumptions for the instrument parameters used. In §3 we present how we calculate the signal to noise ratio of HIRAX to evaluate the instrument's ability to detect

**Table 1.** Summary of Simulation Parameters.

Parameter	Value
Telescope Area, A	20 m <sup>2</sup>
Seeing, $\theta_s$	1.5"
Focal Length, $l_{\text{focal}}$	16.963m
Pixel Size	6.9 $\mu\text{m}$
PSF	17.88 pixels
Dark current	4e <sup>-</sup> /pixel/second
Read noise	3e <sup>-</sup> /pixel/read
Saturation	20000e <sup>-</sup> (80%)
Magnification	1
Number of Transits	3
Transit duration	2 hr

sodium in confirmed exoplanets. In §4 we discuss the results of our simulations and in §5 we conclude.

## 2. MODELS AND INSTRUMENT PARAMETERS

Here we describe the instrument parameters and the model spectra used in the calculations of the HIRAX signal to noise ratio (SNR). We also discuss the choice of HIRAX bandpass configurations to consider.

### 2.1. Instrument setup

For the following simulations, we assume the parameters of the Hale telescope at Palomar and typical observing conditions. For the camera we consider CCD noise properties for an off-the-shelf device and assume the pixels fill to 80% of full well before having to read out the exposure. In addition, we assume a total of 3 transits each being 2 hr long. The detailed specifications and setup are tabulated in Table 1. The PSF was calculated using  $\text{psf} = \frac{\theta_s \cdot l_{\text{focal}} \cdot \text{magnification}}{206265 \cdot \text{size}_{\text{pixel}} \cdot 10^{-6}}$ .

### 2.2. Model spectra

The model spectra that were used for the simulations, shown in Figure 4, were stellar spectra from the PHOENIX Library (Husser et al. 2013), Exoplanet spectra from the Goyal’s Library (Goyal et al. 2020), telluric spectra which characterizes the Earth’s atmosphere using the Planetary Spectrum Generator (PSG) (Villanueva et al. 2018) and a PSG wrapper<sup>2</sup> that calls the PSG API to generates high resolution telluric spectra, and the HIRAX profiles we generated using a tophat function.

### 2.3. HIRAX Band Configurations

Five bandpass configurations were constructed using tophats and either 3 or 5 bands and starting positions

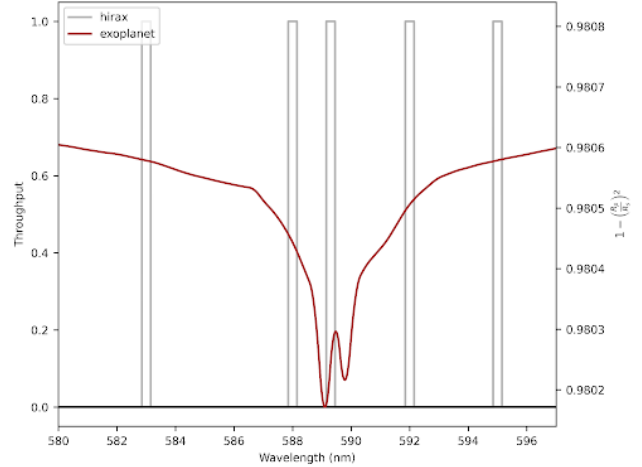


**Figure 3.** HIRAX bandpass configuration plotted over the spectrum of an exoplanet spectrum model. Different configurations are to be tested on this Hot Jupiter’s model spectrum to optimize the band-placements, widths, and throughputs.

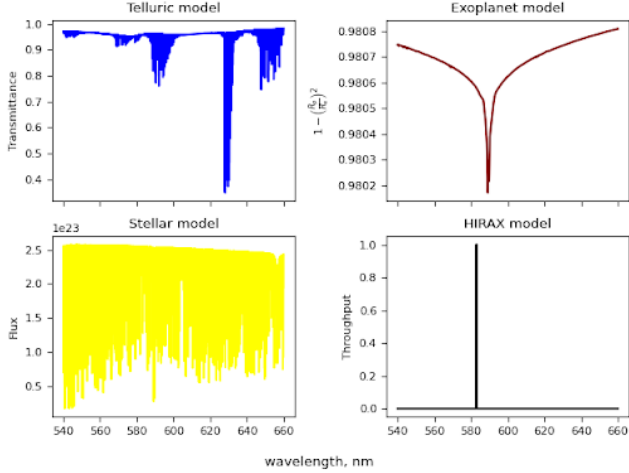
and widths that are consistent with the capabilities of manufacturers (e.g. Alluxa can produce tophat profile filters with widths as narrow as 0.2 nm). As we are looking at Hot Jupiter spectra, our goal was to place bands around the Na doublet present in the atmosphere. Band-placements were roughly centered around 588.995 nm and 589.9524 nm. The different features of the configurations that we were interested in changing are: *the placements of the bands, the width of the bands, and the throughput of the bands*. There is a trade off between widening the bands and their placements closer or further away from each other and with respect to the exoplanet sodium feature. Exploring this trade off in order to determine to optimal bandpass characteristics is the aim of this work. As such, we chose five fairly distinct bandpass setups to do an initial test of the code. Refined bandpass configurations can then be considered later. In choosing the bandpass locations, we also considered telluric absorption and emission, which we discuss below.

Fig. 3 shows a hot Jupiter atmospheric spectrum around the sodium doublet in units of transmission versus wavelength, along with five 0.3 nm width HIRAX bandpasses that have a tophat profile. This is just one example of a bandpass configuration possible for HIRAX.

#### 2.3.1. Considering Tellurics

While deciding where to place the bands around the Na feature, the effect of the telluric spectrum and the OH spectrum had to be taken into account. Ideally the bands would not overlap with these two features but as Figure ?? shows, the tellurics greatly overlap with the

<sup>2</sup> [https://github.com/ashbake/run\\_psg](https://github.com/ashbake/run_psg)



**Figure 4.** The 4 different model spectra that were used throughout these simulations.

bands and are unavoidable as they are at the same wavelength as the doublet we wish to characterize. The OH features however, are much further away and therefore are not a concern for contaminating the measurement.

The planned solution to these unavoidable telluric water vapor absorption features, which are quite variable in time, is to separately monitor them and take into account their effects in the data analysis process of the data. Adding an off-the-shelf spectrometer to the HIRAX design that simultaneously measures water vapor features during a transit observation is currently underway.

### 3. CALCULATING SNR

In this section, we present the different simulations that were carried out to find a first-pass result for measuring the SNR of a sodium detection in the HIRAX bands. The first step in the process is to integrate the flux of the stellar spectrum, scaled to the flux levels expected at the detector based on the star's assumed magnitude and the assumed throughput of HIRAX, over the HIRAX bandpasses. The resulting flux in units of photons/m/s is then multiplied by the Hale area of  $20 \text{ m}^2$  and the exposure time of 2 hours. Eq 1 shows the full equation. The error bars we then determined from the sum in quadrature of the photon, read, and dark noise evaluated given the detector properties. This produces the estimated flux in the HIRAX bandpasses and the expected noise.

$$1 - \left( \frac{R_p}{R_s} \right)^2 = At_{exp} \int f_{stel} f_{exo} f_{tel} f_{hirax} d\lambda \quad (1)$$

We then fit a Lorentz curve to the simulated data, shown in Figure 6, to extract the amplitude and width

of the simulated curves and record them alongside their errors using the fitting. For the rest of the simulations, only the amplitudes are used as signal and the error in the amplitude is used as the error. In the future we also hope to explore the width parameter and the error associated to it. We then calculate the SNR and plot it against different V magnitudes. These plots were made for the five different bandpass configurations. Figure 7 & 8 show the SNR and the most favorable configuration (configuration 5) respectively. The other plots can be found in the appendix. In Figure 7 you can see a configuration with 3 bands 0.3 nm in width all close to the Na doublet wavelength of 588.995 nm and 589.9524 nm. In addition to changing the width and the placements of the bands, we also varied the throughputs for each configuration. As expected the lower the throughput the worse the SNR. However, the purpose of testing out different throughputs was to find whether there is a significant difference in our count of detectable exoplanets to get a more expensive higher throughput instrument and to obtain a lower and higher estimates of how many exoplanets we might be able to detect with our device.

Comparing the plots in 7 and 8 alongside the figures in Appendix A. we find that there is a benefit to widening the bands as this allows more light into the instrument thus reducing the photon noise, which is the limiting noise source. Surprisingly though, the 5th configuration with just 3 bands and narrow 0.3 nm widths is the most favorable in terms of the amplitude constraint. This may be due to how we are performing the fits as we are setting the Lorentz baseline constant, so we will refine this in future work. For example, it would be possible to marginalize over this baseline term as an alternative to keeping it constant.

Next, we run simulations to determine and compare exactly how many exoplanets that are observable from Palomar ( $\text{dec} > -20^\circ$ ) in EU and ARXV catalog can be detected for the 5 different configurations that we are testing. To classify what is observable and what is not, we plot Magnitude vs Differential Transit Signal of 2 atmospheric scale height alongside  $3\sigma$  noise lines taken from the Lorentz fit as shown in Fig. 9 and in the Appendix. The differential transit signal was calculated following Sing (2018) using eq (2), (3) and (4).

$$A = \frac{2R_{pl}H}{R_{st}^2} \quad (2)$$

$$H = \frac{k_B T}{\mu g} \quad (3)$$

$$T = T_{eq} = \left( \frac{1}{4} \right)^{1/4} T_{eff} \left( \frac{R_s t}{a} \right)^{1/2} \quad (4)$$

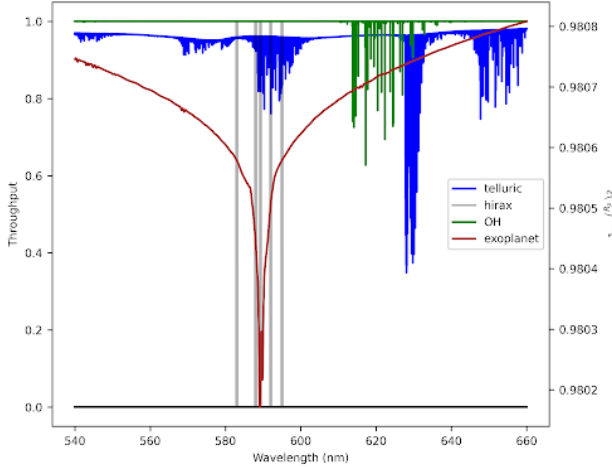


**Figure 5.** Telluric transmittance in blue, OH lines in green, and HIRAX bandpasses under consideration in gray (left axis) and exoplanet transmission spectrum in red (right axis) versus wavelength in nanometers. Figure illustrates significant overlap between the bands and the telluric spectrum.

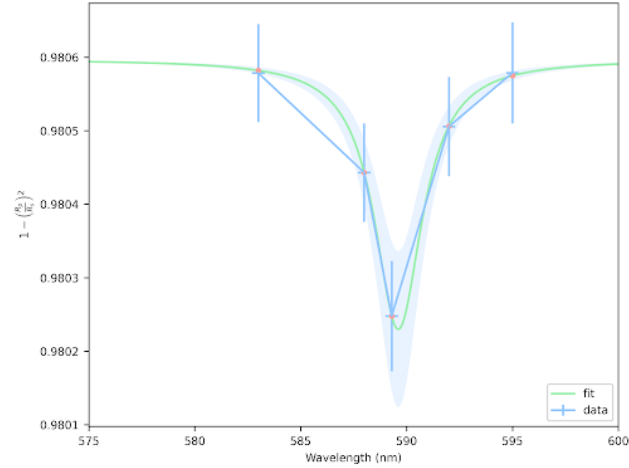


**Figure 6.** Fitting a Lorentz function to our flux ratio plot to determine the parameters used to find the SNR. The Lorentz fit gives us the signal and the noise in our simulations. The amplitude of the Lorentz profile,  $a$ , is associated to the signal and the  $\text{acov}$ , where  $\text{acov}$  is the covariance of the amplitude in the covariance matrix, gives us the error.

We characterized a planet as detectable for a certain throughput if they were above the  $3\sigma$  line at that throughput. We choose  $3\sigma$  here as it is typical detection limit for exoplanet studies; as such our results remain comparable to those of other works.

#### 4. RESULTS AND DISCUSSION

The number of detectable planets is summarized in a bar chart shown in Fig. 10. From the figure we see it is obvious that configuration 5 results in the most de-

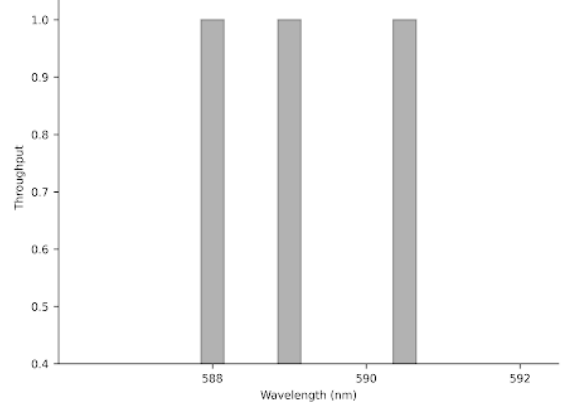


**Figure 7.** HIRAX filter profile with 3 bands of 0.3 nm on the right all close to the Na doublet wavelength at 588.995 nm and 589.9524 nm

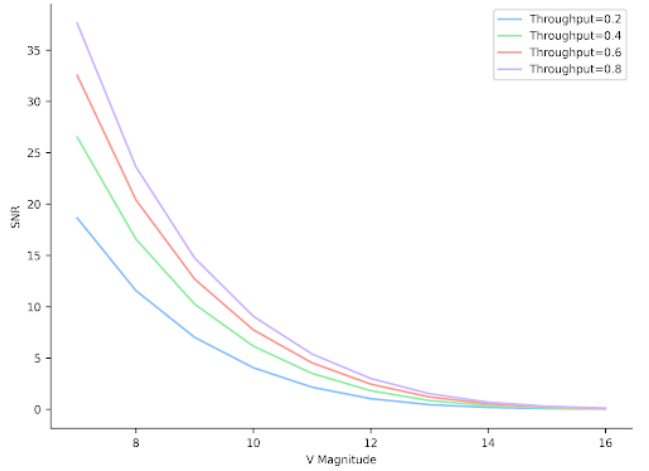


**Figure 8.** SNR vs Magnitude for different throughputs represented by the different vertically shifted lines. The higher throughput settings allow more photons into the detector which results in a much higher signal-to-noise ratio at the same magnitude compared to a lower throughput.

tectable planets throughout all the throughputs. Realistically, a throughput of 0.8 is likely out of reach of the current HIRAX budget. However, the point of determining results for all these throughputs, as mentioned before, was to justify whether a much more expensive camera with a higher throughput would be worth it or an off-the-shelf camera would be good enough. Since we can characterize 14 planets still in configuration 5 for a 20% total throughput, we confirm that a less expensive camera would be sufficient for the first demonstration of HIRAX, until an upgrade later would be possible. It is important to note that this is *not* the final result as much more work is to be done to come to a more refined

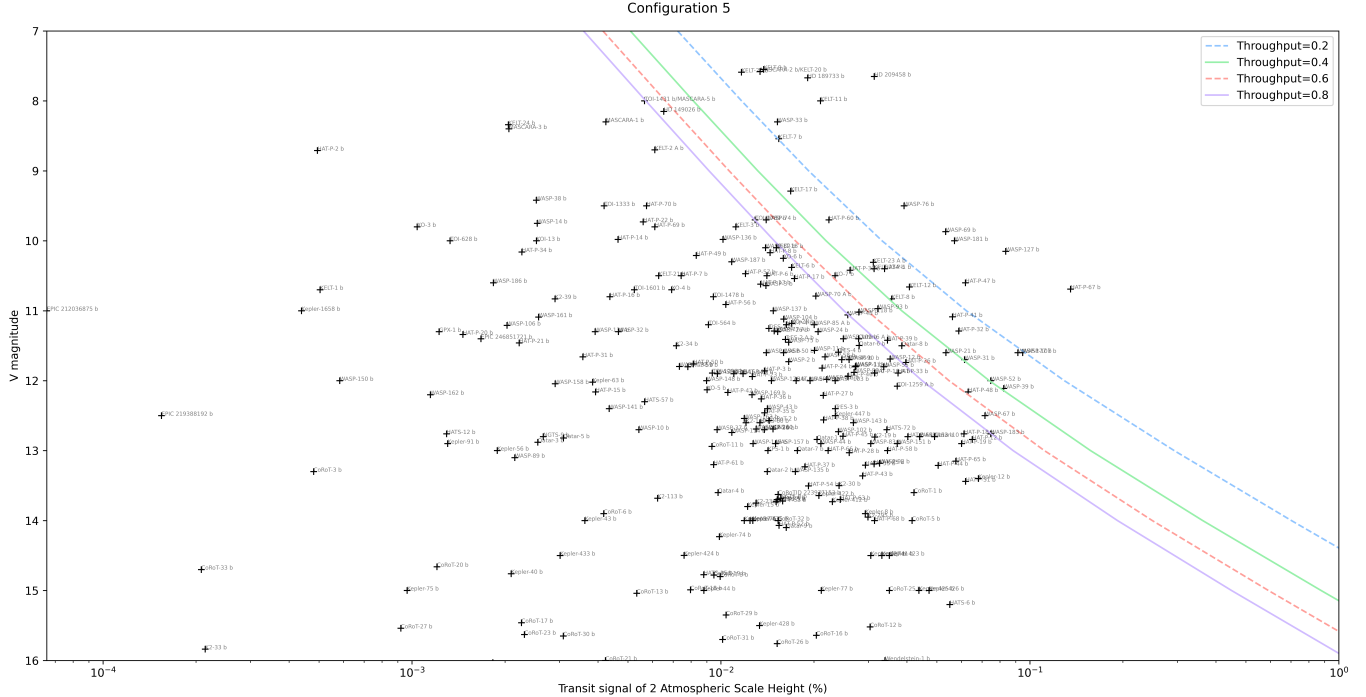


**Figure 9.** Magnitude vs Differential Transit signal of 2 Atmospheric Scale Height (%) with  $3\sigma$  noise lines generated from the model Lorentz fit and Hot Jupiters in the northern hemisphere (declination  $> -20^\circ$ ). Exoplanets to the top right of the  $3\sigma$  are considered detectable.

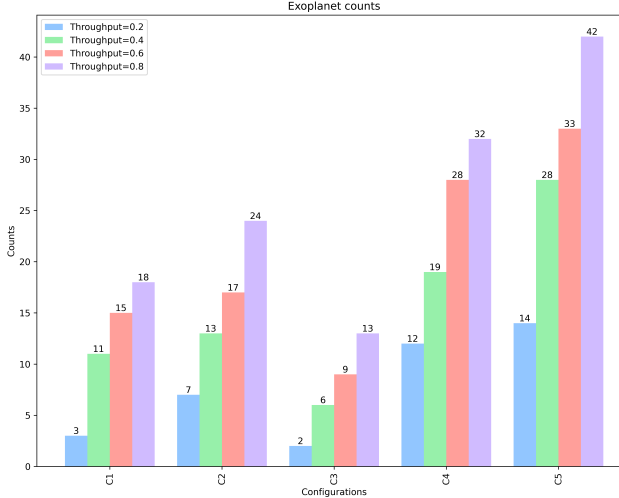


**Figure 10.** Summary of the results of the Lorentz amplitude-fit simulations shown for the 5 different configurations for 4 different throughputs. The vertical axis represents the number of exoplanets that are detectable.

choice of bandpass configuration, particularly from analyzing results of the widths constraints for each bandpass configuration.

#### 4.1. Future Work

As mentioned above, future work will include analyzing the results of the width fits that are already per-

formed here. Alongside this, the code developed for this project will be adapted to look at a few more effects including Doppler shift due to the various velocities in the system. These velocities include that of the exoplanet orbit, stellar radial velocity, and Earth Barycentric velocity, which each will cause the various source and transmission spectra to shift on various timescales. However, whether these shifts are significant enough to change our final choice of band placements is to be tested. An example of how the signal of the exoplanet may change across the HIRAX bandpasses is shown in Fig. 11, where we overplot the HIRAX bandpasses for the first configuration considered. We see some shift in the spectrum as expected. The cores of the sodium doublets shift across the HIRAX bandpasses, but not to a degree that would compromise HIRAX's ability to detect a feature since the shifts are insignificant for the reference bandpasses away from the sodium line cores. It is expected that the rest of the configurations will behave similarly but a more rigorous analysis should be performed for each case.

## 5. CONCLUSIONS

HIRAX is a multiband imager that will be set up in Palomar to characterize the sodium doublet feature in Hot Jupiter atmospheres. We have investigated 5 bandpass configurations and for each present a detectable

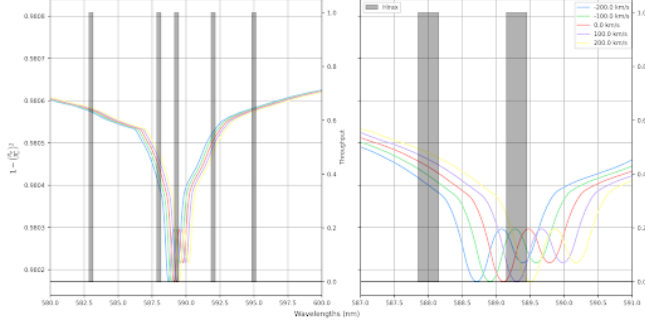


**Figure 11.** Simulated results with the addition of variable Exoplanet motion during transit, Stellar proper motion, and Earth’s Barycentric motion showing the shift in spectrum.

exoplanet count for various throughputs. From this we have tentative results of favorable bandpass placements

and widths for the HIRAX instrument to optimally detect the Na feature. The simulations favor bandpasses that are grouped near the core of the Na doublet, however more work is needed to confirm this result. In particular, the final bandpass configuration chosen requires further investigations into telluric correction, velocity shifts, width fits, and different instrument parameters like read noise, dark noise, magnification and such are required for a final design. In the long term, HIRAX could be used to characterize terrestrial planets with biosignatures such as oxygen, which would be observable from space. The simulations presented here would be easily adaptable to studying this terrestrial application.

## REFERENCES

- Baker, A. D., Blake, C. H., & Halverson, S. 2019, PASP, 131, 064402
- Fisher, C., & Heng, K. 2019, ApJ, 881, 25
- Goyal, J. M., Mayne, N., Drummond, B., et al. 2020, Monthly Notices of the Royal Astronomical Society, 498, 4680–4704. <http://dx.doi.org/10.1093/mnras/staa2300>
- Heng, K. 2016, ApJL, 826, L16
- Husser, T. O., Wende-von Berg, S., Dreizler, S., et al. 2013, A&A, 553, A6
- Knutson, H. A., Dragomir, D., Kreidberg, L., et al. 2014, The Astrophysical Journal, 794, 155. <https://doi.org/10.1088/0004-637x/794/2/155>
- Sing, D. K. 2018, arXiv e-prints, arXiv:1804.07357
- Villanueva, G. L., Smith, M. D., Protopapa, S., Faggi, S., & Mandell, A. M. 2018, JQSRT, 217, 86

## APPENDIX

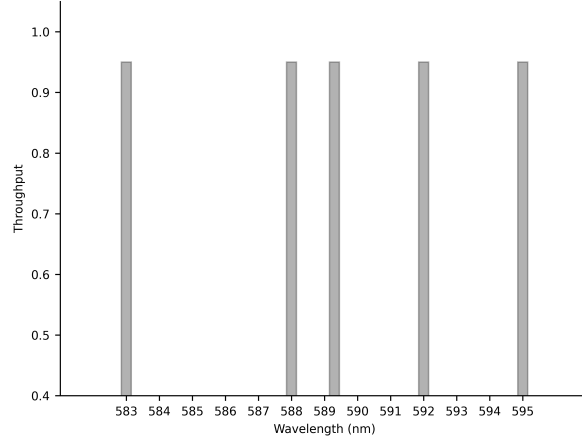


**Figure 12.** HIRAX profile - configuration 1

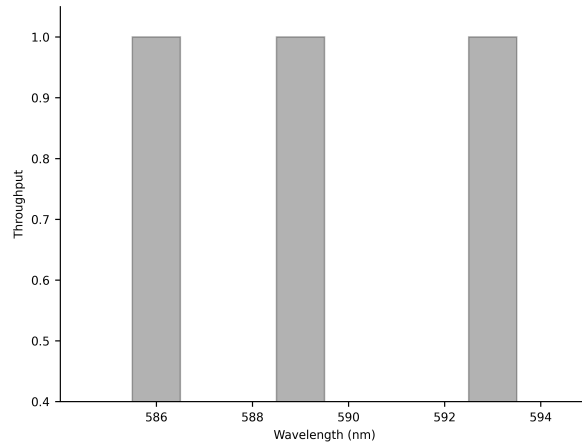


**Figure 13.** HIRAX profile - configuration 2

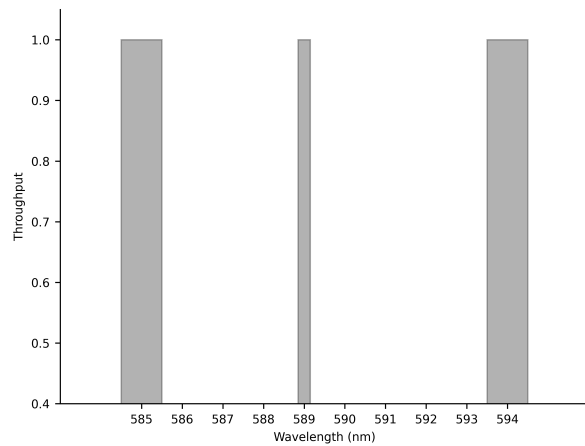


**Figure 14.** HIRAX profile - configuration 3

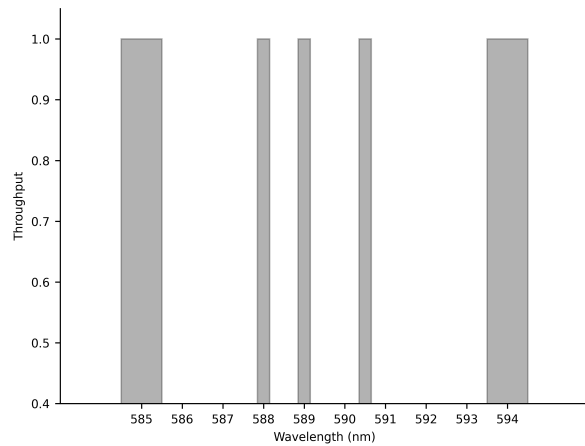


**Figure 15.** HIRAX profile - configuration 4

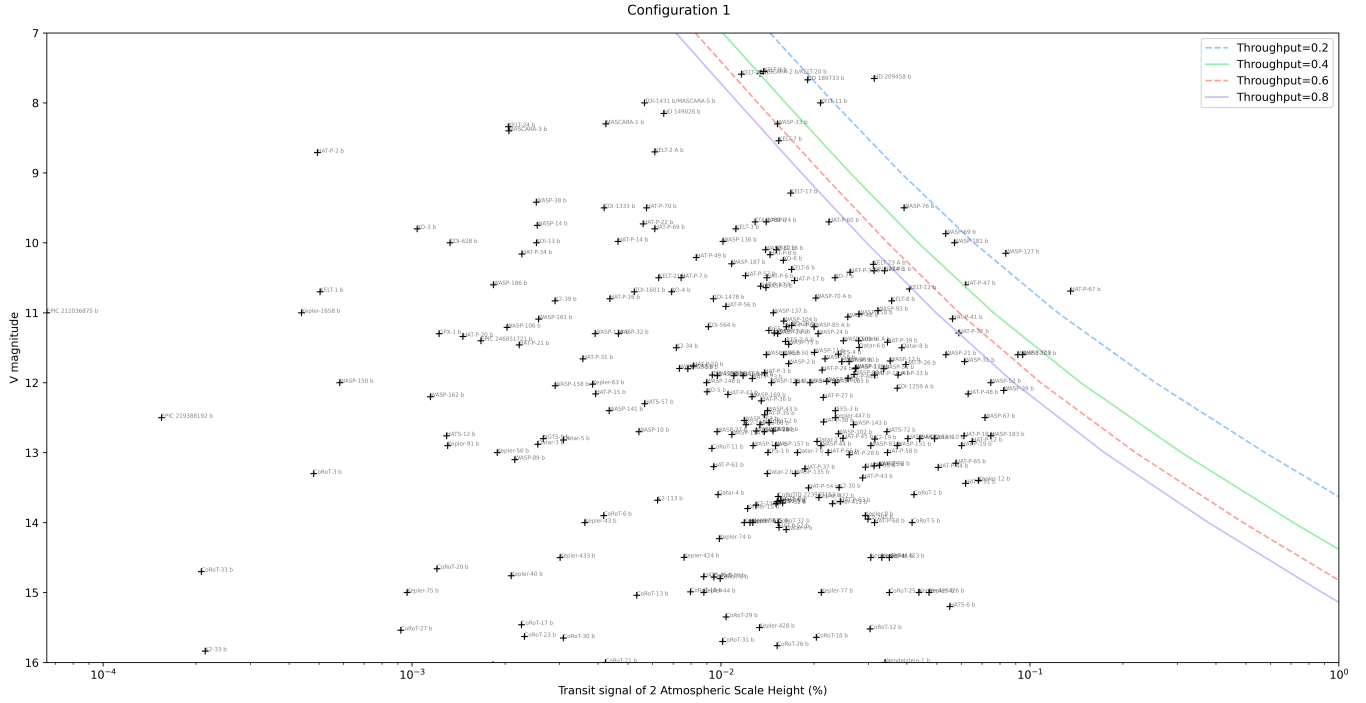


**Figure 16.** VMagnitude vs Transit signal for multiple throughput - configuration 1

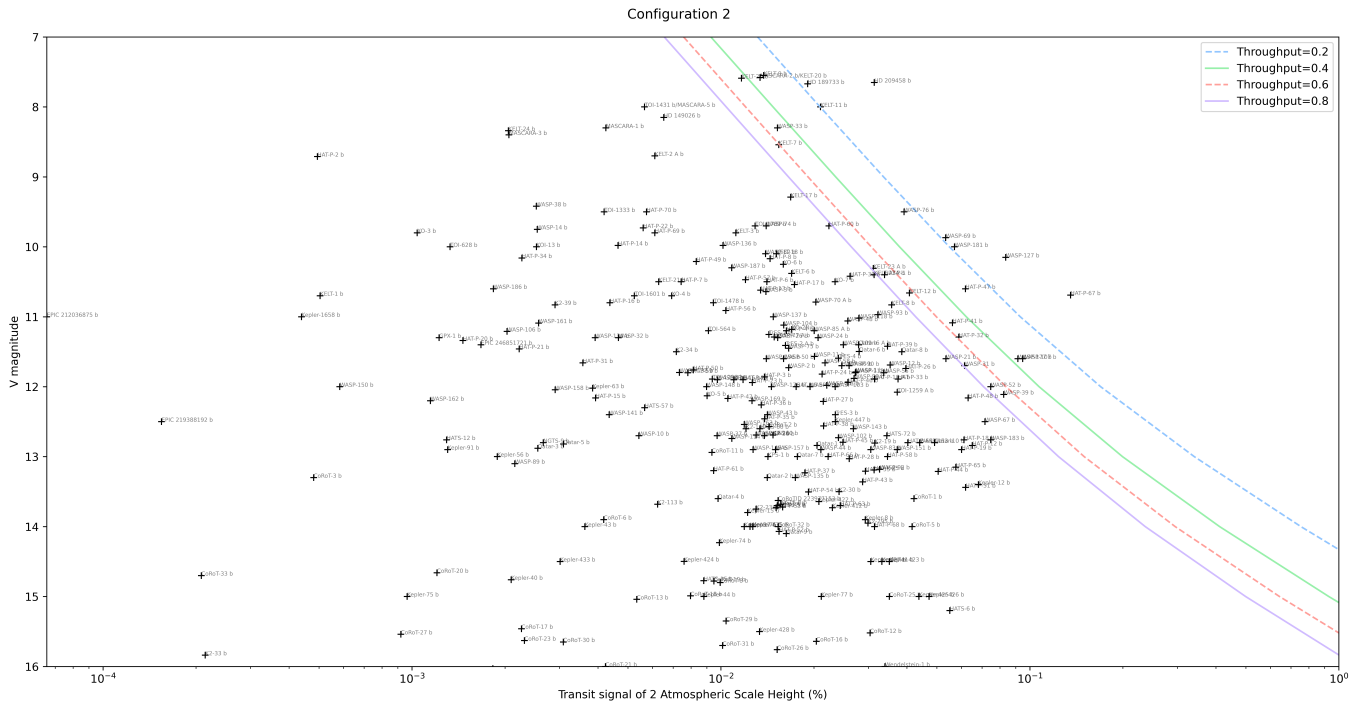


**Figure 17.** VMagnitude vs Transit signal for multiple throughput - configuration 2

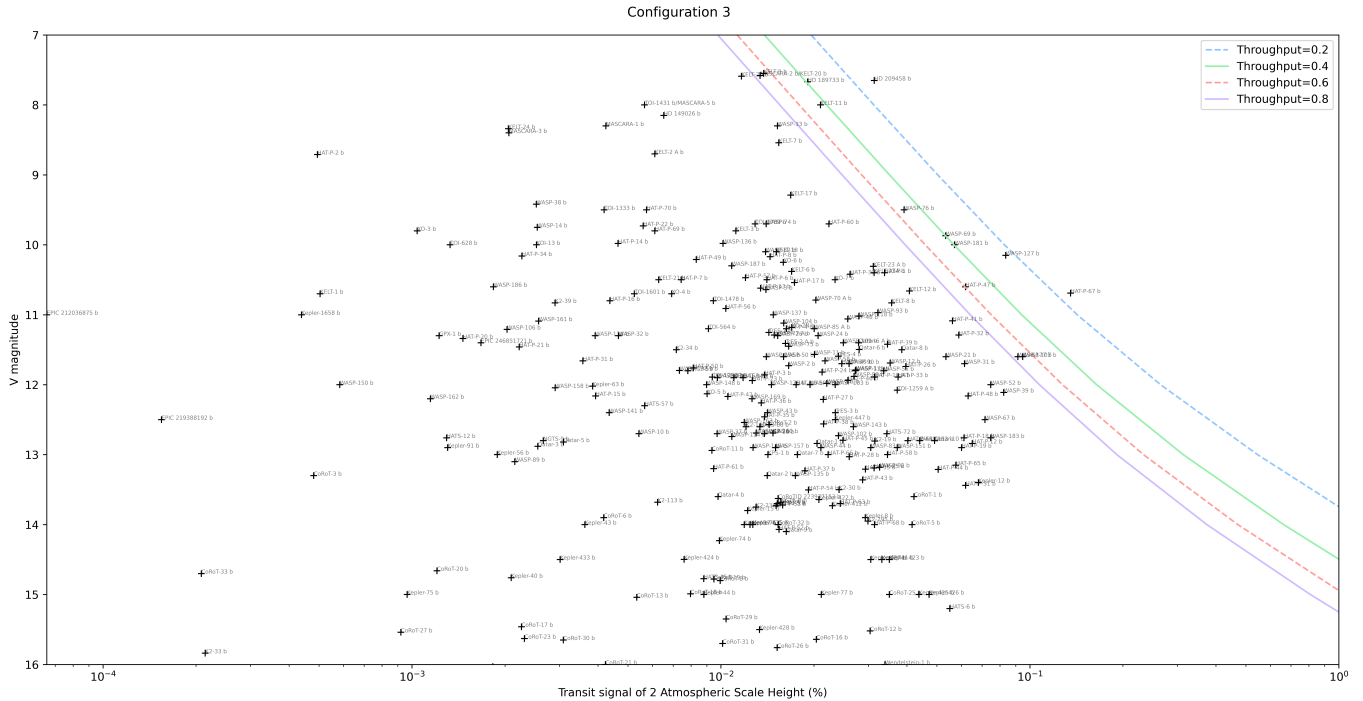


**Figure 18.** VMagnitude vs Transit signal for multiple throughput - configuration 3

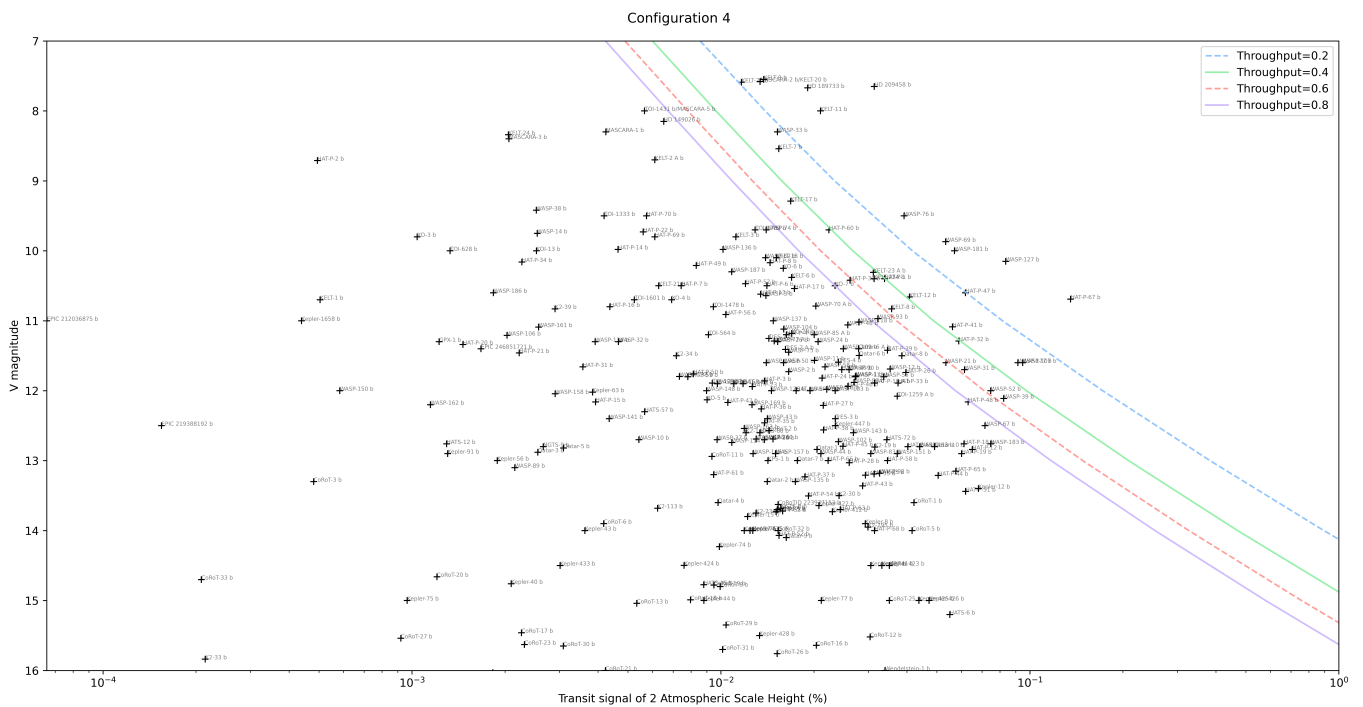


**Figure 19.** VMagnitude vs Transit signal for multiple throughput - configuration 4